Phase transition behavior of heterostructural alloys: Effects of size mismatch and site preference

Yi-Feng Zheng,[1] Peng Zhang,[2] and Su-Huai Wei[1,*]
[1]*Beijing Computational Science Research Center, Beijing 100193, China*
[2]*Shenzhen University, Shenzhen 518060, China*

(Received 12 May 2022; accepted 15 June 2022; published 29 June 2022)

Unlike isostructural alloys, phase transitions of heterostructural alloys between two different lattice types involve more complexity and are less explored. In this work by analyzing the local environment around each atom, we study the distinct features of phase transitions in three prototypical alloy systems (Cd,Pb)Te, (Cd,Ge)Te and (Zn,Mg)O with different size and chemical mismatches. We show that for the (Zn,Mg)O alloy with small size mismatch and low site preference energy between the Zn and Mg compounds, the phase transition occurs abruptly from the zinc-blende to rock-salt structures, showing the feature of a first-order transition. On the contrary, many distorted local configurations unlike either tetrahedron or octahedron ones in the zinc-blende or rock-salt structures, respectively, exist near the phase transition in (Cd,Ge)Te and (Cd,Pb)Te alloys, which have low formation energies. This is attributed to the large size mismatch between CdTe and PbTe, and stronger preference of Cd occupying the tetrahedral sites, whereas Pb and Ge occupying the octahedral sites in (Cd,Pb)Te and (Cd,Ge)Te alloys. Consequently, the phase transitions in (Cd,Pb)Te and (Cd,Ge)Te alloys happen gradually in a wide composition range, showing the feature of a second-order transition. Our study, therefore, shows that phase transition behaviors of heterostructural alloys can be rather complex, either abrupt or gradual, largely depending on the size mismatch and site preference of the constituents. This provides deep understanding on the phase transition behavior of these types of heterostructural alloys.

DOI: 10.1103/PhysRevB.105.214113

I. INTRODUCTION

Alloying semiconductors *AX* with *BX* is a useful approach to tune various material properties, hence, it is widely used in a large variety of applications. Usually, alloying to form *(A,B)X* was done between compound *AX* and *BX* with the same crystal lattice structures because they usually have high miscibility. For instance, mixing InAs and GaAs will form (Ga,In)As in the same zinc-blende structure with band gap varies from 0.4 to 1.5 eV. Extensive studies have been done for these isostructural alloys, focusing mostly on the composition-dependent optical and electronic properties [1,2], morphology of the film surface [3] and atomic ordering induced property changes [4,5]. The studies of alloys where *AX* and *BX* have different lattice types are rare, because there is still lack of knowledge about how the structures of *(A,B)X* evolve with the concentrations of A and B. Early theoretical studies [6] attempted to investigate such heterostructural alloys by assuming that the alloy structures change abruptly from one to the other. For example, ZnO has tetrahedral wurtzite structure but MgO has octahedral rock-salt structure. By calculating the formation energies of (Zn,Mg)O separately in wurtzite and rock-salt lattices, the phase transition was inferred at the composition where the formation energies of the two lattices crosses. As Zn and Mg have similar ionic radii and chemical properties [7,8], the mixing of the two atoms to form alloys is relatively easy and an assumption of direct transition may be reasonable. An abrupt structural transition from cubic to hexagonal phase was indeed observed in experiments [9]. However, similar approaches were also applied to the case of (Cd,Pb)Te [10] where both the ionic sizes and chemical properties of Cd and Pb are rather different. All the calculated alloy structures were assumed to be fixed in either zinc-blende or rock-salt lattices, thus the transition was assumed to be abrupt, jumping directly from zinc-blende to rock-salt lattice or vice versa [10].

Nevertheless, due to the large size and chemical mismatch between Cd and Pb, more complicated structures such as the occupation of both tetrahedral and octahedral sites may occur as the mixing ratio changes because the elements have strong preferences to occupy either tetrahedral or octahedral sites and the large size mismatch can further enhance such preferences. To understand this issue, in this work, we perform systematic studies to investigate whether the alloys will directly change from zinc-blende to rock-salt lattice, showing the feature of a first-order transition, or there may exist intermediate metastable structures unlike either lattice, showing the feature of a second-order transition. We will demonstrate that the type of phase transition in these *(A,B)X* alloys is closely related to the properties of the constituents, such as the lattice mismatch between *AX* and *BX* as well as the site preference energy of the constituents.

The systems we choose to study are (Zn,Mg)O, (Cd,Ge)Te, and (Cd,Pb)Te. They are not only of great theoretical importance, but also have attracted broad interests for possible practical applications. Alloying ZnO with MgO produces tunable high band-gap (Zn,Mg)O alloys [11–13], which are

*suhuaiwei@csrc.ac.cn

widely used in solar-blind ultraviolet photodetectors [14,15] and as buffer layers in thin-film solar cells [16,17]. A similar heterostructural alloy (Zn,Cd)S can also be used as buffer layers in thin-film solar cells [18]. PbTe has been extensive studied as efficient thermoelectric material for decades and alloying Cd to form (Cd,Pb)Te [19,20] has the potential to tune its band structure [21] and enhance the thermoelectric figure of merit [22]. Understanding how the structure evolves as function of Cd composition will provide insight for a better control of the alloy properties. Moreover, we also include (Cd,Ge)Te [23] to compare the influence when Pb is replaced by Ge, which has a more similar size as Cd but GeTe has a higher site preference to be at octahedral site.

The structure of this paper is as follows. In Sec. II, we describe the computational methods used in this work. Section III A compares the material properties of the constituents. Section III B presents the phase transition in the simple alloy system of (Zn,Mg)O. Section III C demonstrates how the formation energies and coordination numbers change with compositions in more complicated alloy systems of (Cd,Pb)Te and (Cd,Ge)Te. Finally, the influence of lattice mismatch and site preferences of atoms on phase transition behaviors are discussed and a conclusion is given in Sec. IV.

II. COMPUTATIONAL METHODS

The structures of alloys are generated using the cluster expansion method as implemented in the Alloy Theoretic Automated Toolkit (ATAT) [24,25]. The generated alloy structures contains various distributions of atoms, e.g., in the zinc-blende structure of (Cd,Pb)Te, the zinc-blende sublattice sites for cations are occupied by either Cd or Pb, and various possibilities are included in these generated structures. The numbers of alloy structures we use for each alloy system is around 100, which is automatically generated by the ATAT code with the cross validation score around few meV. The supercells of alloys we used in this study are 64-atom cell or less. The total energy calculations are performed using the Vienna ab-initio simulation package (VASP) [26,27]. Projector augmented-wave method [28,29] is adopted for the pseudopotentials, and Perdew-Burke-Ernzerhof functional [30] is adopted for the exchange-correlation functional. The energy cutoff for the plane wave basis is 500 eV, and all atoms are relaxed until the forces on each atom fall below 0.01 eV/Å.

For this study, it is important to know the coordination of the atoms to analyze the bonding characters and determine whether they should be classified as zinc-blende, rock-salt or mixed. To do this, we first categorize the atoms into cations and anions, and then define the coordination number of each atom by the number of surrounding atoms of different types. Take one Cd in (Cd,Pb)Te as an example, we search its nearest-neighboring atoms by gradually increasing the radius, accepting the atom as its coordination atom if it is Te atom, till we meet a cation like Cd or Pb, then we count how many Te atoms are within this dynamic radius as the coordination number for this particular Cd atom. Such procedures are applied to all atoms, and the average coordination number for this alloy structure is assigned for the cation and anion. Obviously, the average coordination number for the standard zinc-blende lattice is 4, and the number becomes 6 for the rock-salt lattice. For those structures with average coordination numbers between 4 and 6, typically around 5, we denote them as distorted structures.

It is interesting to point out that the determination of coordination numbers for structural identifications is not a simple task and various approaches have been used in the past [31]. The conventional method [32] usually requires an input of fixed cutoff radius for searching coordination neighbors for given atoms, which is somewhat ambiguous, especially for systems with large atomic displacements where it is hard to choose a suitable cutoff. In contrast, the system we studied here has well defined cation-anion bonds and the formation of anion-anion or cation-cation bonds has a high formation energy, so our dynamic radius searching method for coordination numbers is more natural and efficient, which avoids the arbitrariness that occurred in previous approaches.

III. RESULTS AND DISCUSSIONS

A. Material properties of the constituents

In this work, we focus on the phase transition behaviors between zinc-blende and rock-salt types of alloys, taking (Cd,Pb)Te, (Cd,Ge)Te, and (Zn,Mg)O as three examples. ZnO normally has wurtzite structure, but the energy difference between the tetrahedral wurtzite and zinc-blende phases are negligible compared with the one with the rock-salt structure, so for this theoretical study, we treat ZnO as having the zinc-blende structure. To study the formation of alloys, it is instructive to first explore the properties of the end-point binary constituents. Table I lists the lattice constants of the corresponding binary constituents in both lattice structures, and the energy differences between the rock-salt and zinc-blende structures. Positive energy indicates the zinc-blende structure is more stable. It is obvious that the lattice constants of MgO and ZnO are quite close, both in zinc-blende and rock-salt lattices, as Mg and Zn have similar ionic and covalent sizes. Therefore, it is expected that (Zn,Mg)O alloy can be easily synthesized. On the contrary, a large lattice mismatch always exists between CdTe and PbTe in both lattices, while the lattice constant mismatches between CdTe and GeTe are relatively small.

TABLE I. Cubic lattice constants a of the end-point binary compounds in both zinc-blende (ZB) and rock-salt (RS) lattices, and the energy differences per unit formula ΔE between the rock-salt and zinc-blende structures. Positive ΔE indicates the ZB structure is more stable. The numbers in the parentheses denote the deviations of lattice constants from the reference compounds. ZB PbTe and GeTe are referenced to ZB CdTe, and ZB MgO is referenced to ZB ZnO. The same reference compounds are chosen for the RS structures, respectively.

Binary	a_{ZB} (Å)	a_{RS} (Å)	ΔE (eV)
CdTe	6.624 (0%)	6.132 (0%)	0.361
PbTe	7.336 (10.7%)	6.566 (7.1%)	−0.378
GeTe	6.759 (2.0%)	6.007 (−2.0%)	−0.465
ZnO	4.628 (0%)	4.335 (0%)	0.286
MgO	4.607 (−0.5%)	4.246 (−2.1%)	−0.210

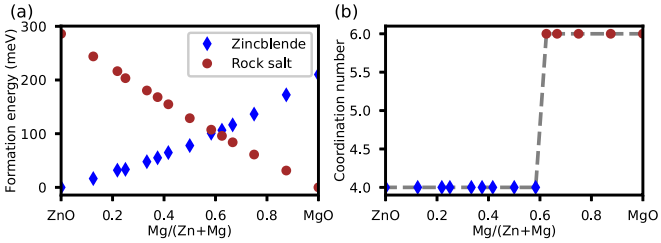

FIG. 1. The formation energies (a) and coordination numbers (b) of (Zn,Mg)O alloys. Blue diamonds denote zinc-blende structures, and brown circles denote rock-salt structures. The abscissa represents the concentration of Mg. Only those with the lowest formation energies in the zinc-blende and rock-salt structures are presented in (a), and no distorted structures appear. For coordination numbers, only the one with the lowest formation energy at each concentration is presented in (b). Obviously, the phase transition of (Zn,Mg)O alloys shown here is abrupt and hence a first-order transition.

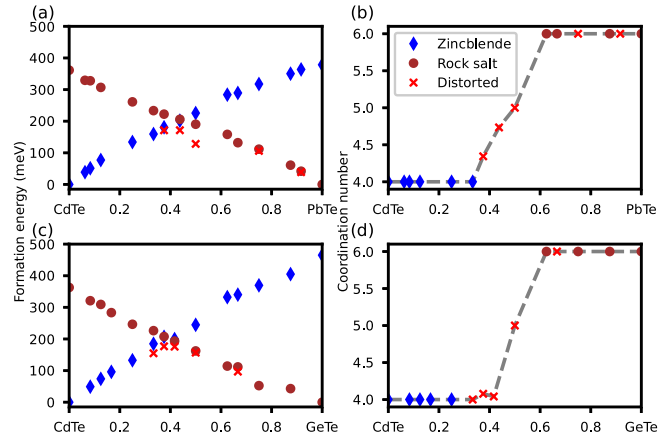

FIG. 2. The formation energies and coordination numbers of (Cd,Pb)Te (a), (b) and (Cd,Ge)Te (c), (d) alloys. Blue diamonds denote zinc-blende structures, brown circles denote rock-salt structures, and red crosses denote distorted structures. The abscissa represents the composition of Pb or Ge. Only those with the lowest formation energies in the zinc-blende and rock-salt structures are presented, and distorted structures are only shown when the formation energy is the lowest at that component concentration. For coordination numbers, only the one with the lowest formation energy at each concentration is presented. In both alloys, there exist distorted structures with lower formation energies than in either lattice, hence the phase transitions happen gradually in a wide composition range, showing the feature of a second-order transition.

The energy differences between the rock-salt and zinc-blende structures are comparatively small for ZnO and MgO. In contrast, such energy differences become large for CdTe, PbTe, and GeTe, indicating that Cd has high preference to be at the tetrahedral site, whereas Pb and Ge prefer to be at the octahedral site. As will be discussed in the next section, the lattice mismatch as well as site preferences of atoms plays important roles in the alloy formation and phase transition behaviors.

B. Abrupt phase transitions in (Zn,Mg)O alloys

To exhibit the phase transition in a straightforward manner, the variation of formation energies and coordination number as a function of alloy composition x for (Zn,Mg)O alloys is depicted in Fig. 1. The formation energies of alloys are based on the common reference, i.e., the energies of the most stable structures of the two end-point constituents. Therefore, the formation energy of $Zn_{1-x}Mg_xO$ is given by

$$\Delta H(Zn_{1-x}Mg_xO) = E(Zn_{1-x}Mg_xO) - (1-x)E_{ZB}(ZnO) - xE_{RS}(MgO),$$

where $E_{ZB}(ZnO)$ is the energy of zinc-blende ZnO, and $E_{RS}(MgO)$ is the energy of rock-salt MgO. For each Mg concentration, the lowest formation energies of alloys in the zinc-blende, rock-salt and distorted structures are presented, respectively, and the distorted structures will only be shown when the formation energy is the lowest at that component concentration. Phase transitions are evident from the crossing of formation energies in the two lattices, and also from the abrupt change of coordination numbers. The evident distinction in the phase transition of (Zn,Mg)O alloys is that no distorted structures appear. As the concentration of Mg increases to be near 0.6, the alloy changes abruptly from the zinc-blende structure to rock-salt structure, showing an evident feature of a first-order transition. Moreover, the trend of how the formation energy in each lattice varies with the concentration of Mg is almost linear with, slightly downward bowing. This is because the lattices of MgO and ZnO match well, both in zinc-blende and rock-salt structures, and hence the strain energy cost in forming alloys is small. The electronegativity difference of Mg and Zn causes charge transfer and lower the formation energies, therefore, alloy mixing in (Zn,Mg)O alloys is slightly favored in each individual lattice for this lattice-matched semiconductor alloys. For this system, the energy difference between zinc-blende and rock-salt phases is small, indicating that Zn and Mg are not very sensible to either tetrahedral or octahedral sites. Consequently, (Zn,Mg)O alloys can exist in both zinc-blende or rock-salt lattices without large distortions.

C. Gradual phase transitions in (Cd,Pb)Te and (Cd,Ge)Te alloys

Unlike the simple phase transitions in (Zn,Mg)O alloys, the situations in (Cd,Pb)Te and (Cd,Ge)Te alloys are more complicated. Following the same analyzing methods, we present the corresponding formation energies and coordination numbers in Fig. 2. In contrast to the abrupt phase transition of (Zn,Mg)O alloys from zinc-blende to rock-salt, there exist distorted structures with lower formation energies in (Cd,Pb)Te and (Cd,Ge)Te alloys. Generally, the formation energies of these distorted alloys can span a wide range between zinc-blende and rock-salt types, and some highly distorted ones can even be more energetically favored over either type. The change of coordination numbers also reveals the same trend of phase transitions. Both in (Cd,Pb)Te and (Cd,Ge)Te alloys, the coordination number does not jump abruptly from 4 to 6, and intermediate coordination numbers appear near the phase transition. Therefore, we conclude that the phase transitions in (Cd,Ge)Te and (Cd,Pb)Te alloys happen gradually in a wide composition range, showing the feature of a second-order transition.

TABLE II. The average coordination numbers of Cd, Te, Pb, and Ge separately, for the distorted structure (Cd,Pb)Te or (Cd,Ge)Te at 50% concentration. The overall average coordination numbers are also shown.

Alloy	Average	Cd	Pb/Ge	Te
(Cd,Pb)Te	5.0	4.0	6.0	5.0
(Cd,Ge)Te	5.0	4.6	5.4	5.0

More careful investigations also reveal that there are some differences between (Cd,Pb)Te and (Cd,Ge)Te alloys. The most obvious distinction lies in the region near the phase transition in (Cd,Pb)Te alloy, i.e., many distorted structures have apparent lower formation energies than those in the zinc-blende or rock-salt lattices. The reduction of the formation energy is not that evident in (Cd,Ge)Te alloy. This could be explained by the lattice mismatches between the two systems as shown in Table I. Large lattice mismatch between CdTe and PbTe in either zinc-blende or rock-salt lattices induces large lattice distortions and structural relaxations in (Cd,Pb)Te alloys. Particularly, near the phase transition region where the concentrations of Cd and Pb are similar, so the effect of site preference energy is the highest, the atomic structures can be quite different from either lattice types and significant structural relaxations can effectively lower the formation energies, leading to the appearance of more low-energy intermediate structures. Such differences of structural changes between (Cd,Pb)Te and (Cd,Ge)Te alloys are reflected in their coordination numbers. The evident phase transition in (Cd,Ge)Te starts at the Ge concentration of 0.42, and ends at 0.63 as inferred from the steep change of coordination numbers in Fig. 2(d). As for (Cd,Pb)Te, the evident phase transition in (Cd,Ge)Te starts at the Pb concentration of 0.33, and ends at 0.63. The wider phase transition range and more profound structural relaxation in (Cd,Pb)Te than that in (Cd,Ge)Te is consistent with the larger size mismatch in (Cd,Pb)Te alloys.

To further investigate the distorted structures in (Cd,Pb)Te and (Cd,Ge)Te alloys near the phase transition regions, we present the average coordination numbers of Cd, Te, Pb, and Ge separately in Table II. The selected distorted structures have the Pb or Ge concentration of $x = 0.5$, which is near the center of phase transition. The general trend is that Cd prefers to have the coordination number of 4, Pb or Ge prefers to be 6, and Te stays in the middle. It is easy to notice the large difference of coordination numbers between Cd and Pb in (Cd,Pb)Te at $x = 0.5$, as the structural relaxations there are more significant. Since the coordination number of Cd is 4 in the tetrahedral zinc-blende CdTe and the coordination number of Pb is 6 in the octahedral rock-salt PbTe, the site preferences of Cd and Pb in this distorted (Cd,Pb)Te structure are fully satisfied. In contrast, the coordination numbers of Cd and Ge in (Cd,Ge)Te do not differ so obviously at $x = 0.5$ because the structural relaxations there are small. In this case, the site preferences of Cd and Ge are only partially satisfied. These results indicate that the size mismatch strongly influences the structural relaxations and the site preferences of the atoms persist in the distorted structures.

IV. CONCLUSIONS

In this work, we studied the phase transition properties of three alloy systems (Zn,Mg)O, (Cd,Ge)Te, and (Cd,Pb)Te as functions of alloy compositions. We propose a method for calculating the atomic coordination by counting the nearest-neighbor bonds between cations and anions, which provides a convenient and unambiguous way to extract the structural features of largely distorted semiconductor alloys. We illustrated the distinct features of phase transitions in these three systems and attributed the differences to their lattice and chemical mismatches of the constituents. The lattice mismatch between ZnO and MgO is small in both zinc-blende and rock-salt structures, thus, (Zn,Mg)O shows the feature of a first-order transition. In contrast, the size and chemical mismatches between Cd, Ge, and Pb are large, especially between Cd and Pb, thus, (Cd,Ge)Te and (Cd,Pb)Te show the feature of a second-order transition, where the alloys exhibit large atomic distortions near the phase transition regions with lower formation energies and intermediate coordination numbers. Our studies, therefore, demonstrate that heterostructural alloys can exhibit rather different features during phase transitions, where the lattice mismatch of the constituent binary compounds, as well as the site preferences of the atoms are the main influencing factors that determines the phase transition behaviors of the alloys.

ACKNOWLEDGMENTS

This work was supported by the National Natural Science Foundation of China (Grants No. 12088101, No. 11991060, and No. U1930402). The computational resources are provided by Beijing Computational Science Research Center and Beijing Super Cloud Computing Center.

[1] S.-H. Wei and A. Zunger, Giant and Composition-Dependent Optical Bowing Coefficient in GaAsN Alloys, Phys. Rev. Lett. **76**, 664 (1996).

[2] S. H. Wei, L. G. Ferreira, J. E. Bernard, and A. Zunger, Electronic properties of random alloys: Special quasirandom structures, Phys. Rev. B **42**, 9622 (1990).

[3] F. Zha, Q. Zhang, H. Dai, X. Zhang, L. Yue, S. Wang, and J. Shao, The scanning tunneling microscopy and spectroscopy of $GaSb_{1-x}Bi_x$ films of a few-nanometer thickness grown by molecular beam epitaxy, J. Semicond. **42**, 092101 (2021).

[4] S.-H. Wei and A. Zunger, Band gaps and spin-orbit splitting of ordered and disordered $Al_xGa_{1-x}As$ and $GaAs_xSb_{1-x}$ alloys, Phys. Rev. B **39**, 3279 (1989).

[5] S.-H. Wei and A. Zunger, Optical properties of zinc-blende semiconductor alloys: effects of epitaxial strain and atomic ordering, Phys. Rev. B **49**, 14337 (1994).

[6] M. Sanati, G. L. W. Hart, and A. Zunger, Ordering tendencies in octahedral MgO-ZnO alloys, Phys. Rev. B **68**, 155210 (2003).

[7] R. Shannon, Revised effective ionic radii and systematic studies of interatomic distances in halides and chalcogenides, Acta Crystallogr. Sect. A **32**, 751 (1976).

[8] A. L. Allred, Electronegativity values from thermochemical data, J. lnorg. Nucl. Chem. **17**, 215 (1961).

[9] P. Bhattacharya, R. R. Das, and R. S. Katiyar, Fabrication of stable wide-band-gap ZnO/MgO multilayer thin films, Appl. Phys. Lett. **83**, 2010 (2003).

[10] M. Bukała, P. Sankowski, R. Buczko, and P. Kacman, Structural and electronic properties of $Pb_{1-x}Cd_xTe$ and $Pb_{1-x}Mn_xTe$ ternary alloys, Phys. Rev. B **86**, 085205 (2012).

[11] A. Ohtomo, M. Kawasaki, T. Koida, K. Masubuchi, H. Koinuma, Y. Sakurai, Y. Yoshida, T. Yasuda, and Y. Segawa, $Mg_xZn_{1-x}O$ as a II–VI widegap semiconductor alloy, Appl. Phys. Lett. **72**, 2466 (1998).

[12] T. Minemoto, T. Negami, S. Nishiwaki, H. Takakura, and Y. Hamakawa, Preparation of $Zn_{1-x}Mg_xO$ films by radio frequency magnetron sputtering, Thin Solid Films **372**, 173 (2000).

[13] D.-J. Qiu, H.-Z. Wu, N.-B. Chen, and T.-N. Xu, Characterizations of cubic ZnMgO films grown on Si(111) at low substrate temperature, Chin. Phys. Lett. **20**, 582 (2003).

[14] Y. N. Hou, Z. X. Mei, Z. L. Liu, T. C. Zhang, and X. L. Du, $Mg_{0.55}Zn_{0.45}O$ solar-blind ultraviolet detector with high photoresponse performance and large internal gain, Appl. Phys. Lett. **98**, 103506 (2011).

[15] Z. Wang, J. Lin, X. Wei, W. Zheng, and Q. Hu, a solar-blind ultraviolet photodetector with Graphene/MgZnO/GaN vertical structure, Front. Mater. **8**, 787613 (2021).

[16] T. Ablekim, C. Perkins, X. Zheng, C. Reich, D. Swanson, E. Colegrove, J. N. Duenow, D. Albin, S. Nanayakkara, M. O. Reese, T. Shimpi, W. Sampath, and W. K. Metzger, Tailoring MgZnO/CdSeTe interfaces for photovoltaics, IEEE J. Photovolt. **9**, 888 (2019).

[17] M. Nakamura, K. Yamaguchi, Y. Kimoto, Y. Yasaki, T. Kato, and H. Sugimoto, Cd-Free $Cu(In, Ga)(Se, S)_2$ thin-film solar cell with record efficiency of 23.35%, IEEE J. Photovolt. **9**, 1863 (2019).

[18] Y. Xue, S. Zhang, D. Song, L. Zhang, X. Wang, L. Wang, and H. Sun, Effect of concentration of cadmium sulfate solution on structural, optical and electric properties of $Cd_{1-x}Zn_xS$ thin films, J. Semicond. **42**, 112101 (2021).

[19] Y. Pei, A. D. LaLonde, N. A. Heinz, and G. J. Snyder, High thermoelectric figure of merit in PbTe alloys demonstrated in PbTe–CdTe, Adv. Energy Mater. **2**, 670 (2012).

[20] A. A. Azab, A. A. Ward, G. M. Mahmoud, E. M. El-Hanafy, H. El-Zahed, and F. S. Terra, Structural and dielectric properties of prepared PbS and PbTe nanomaterials, J. Semicond. **39**, 123006 (2018).

[21] S. Cai, S. Hao, Z.-Z. Luo, X. Li, I. Hadar, T. P. Bailey, X. Hu, C. Uher, Y.-Y. Hu, C. Wolverton, V. P. Dravid, and M. G. Kanatzidis, Discordant nature of Cd in PbSe: Off-centering and core–shell nanoscale CdSe precipitates lead to high thermoelectric performance, Energ. Environ. Sci. **13**, 200 (2020).

[22] K. Ahn, M.-K. Han, J. He, J. Androulakis, S. Ballikaya, C. Uher, V. P. Dravid, and M. G. Kanatzidis, Exploring resonance levels and nanostructuring in the PbTe−CdtT system and enhancement of the thermoelectric figure of merit, J. Am. Chem. Soc. **132**, 5227 (2010).

[23] E. Dichi, G. Morgant, and B. Legendre, Study of the ternary system cadmium-germanium-tellurium: Phase equilibria in the ternary system, J. Alloys Compd. **217**, 193 (1995).

[24] A. van de Walle, M. Asta, and G. Ceder, The alloy theoretic automated toolkit: a user guide, Calphad **26**, 539 (2002).

[25] A. van de Walle and G. Ceder, Automating first-principles phase diagram calculations, J. Phase Equilib. **23**, 348 (2002).

[26] G. Kresse and J. Furthmüller, Efficiency of *ab initio* total energy calculations for metals and semiconductors using a plane-wave basis set, Comp. Mater. Sci. **6**, 15 (1996).

[27] G. Kresse and J. Furthmüller, Efficient iterative schemes for *ab initio* total-energy calculations using a plane-wave basis set, Phys. Rev. B **54**, 11169 (1996).

[28] P. E. Blöchl, Projector augmented-wave method, Phys. Rev. B **50**, 17953 (1994).

[29] G. Kresse and D. Joubert, From ultrasoft pseudopotentials to the projector augmented-wave method, Phys. Rev. B **59**, 1758 (1999).

[30] J. P. Perdew, K. Burke, and M. Ernzerhof, Generalized Gradient Approximation Made Simple, Phys. Rev. Lett. **77**, 3865 (1996).

[31] D. Faken and H. Jónsson, Systematic analysis of local atomic structure combined with 3D computer graphics, Comp. Mater. Sci. **2**, 279 (1994).

[32] A. Stukowski, Visualization and analysis of atomistic simulation data with OVITO–the open visualization tool, Modell. Simul. Mater. Sci. Eng. **18**, 015012 (2009).